Supplementary Materials

GCaMP6 and Chemogenetic DREADD expression

All mice were maintained at the University of Pennsylvania Perelman School of Medicine John Morgan animal facility with controlled temperature and humidity conditions and had free access to food and water/CORT water. All animal handling was in accordance with guidelines set forth by the School of Medicine's Institutional Animal Care and Use Committee (approved protocol no. 807237).

The genetically encoded calcium indicator GCaMP6f was used for calcium imaging of pyramidal neurons and interneurons in the cortex. GCaMP6f expression was performed using intracranial AAV injections of neonates. Pyramidal neurons were labeled using recombinant AAV9-*CaMKII*-Cre (Addgene, 105558) and AAV9-*CAG*-FLEX-GCaMP6f (Addgene, 100835) or AAV9-*hSyn1*-FLEX-GCaMP6f (Addgene, 100833); 10-100 nL of AAV per mouse). For sparse labeling of pyramidal neurons, we performed serial dilutions of Cre virus in artificial cerebral spinal fluid (aCSF)/fast-green dye (Sigma Aldrich, F725) solution followed by mixing with GCaMP6f and tdTomato viruses. The final injected AAV mix contained 80 % GCaMP virus, ~17.5 % tdTomato virus, and ~2.5 % Cre virus/fast-green dye. A glass micropipette (Drummond, 50001001X10) was pulled and beveled. A plunger was lightly oiled and inserted into the micropipette to pull the AAV mix. Subsequently, pups at postnatal day 1-2 were anesthetized by hypothermia (typically ~ 2-3 min on ice) and the micropipette was used (freehand) to penetrate the skin and skull and deliver ~200 nL of the virus mix. Medial prefrontal cortical (PFC) injections site was determined using landmarks – skull suture lines and head veins – as reference points (fig. S3). In Fig. 1 and 5, GCaMP6f expression was driven using AAV in *Rbp4*-Cre (GENSAT project at Rockefeller University, *Tlx3*-Cre (GENSAT; PL56), *Colgalt2*-Cre (GENSAT; NF107), 031125), *PV*-IRES-Cre (Jackson Laboratory, 008069), *Sst*-IRES-Cre (Jackson Laboratory, 013044) and *VIP*-IRES-Cre (Jackson Laboratory, 010908) mice using neonatal injection technique. Cre-expressing mice were genotyped for the presence of Cre based on established protocols as an adult. Imaging was performed in 1 to 2-month-old mice, using both sexes, after at least 4 weeks of AAV expression. Mice were group-housed in temperature and humidity-controlled rooms on a 12-hour light/dark cycle after injections.

DREADD-induced modulation of cell types.

Layer 5 (L5) pyramidal neuron and cell type specific interneuron modulation was accomplished with expression of Cre-dependent DREADD-$hM_3D(G_q)$ (AAV9-*hSyn1*-DIO-$hM_3D(G_q)$-mCherry; Addgene, 44361) or $hM_4D(G_i)$ (AAV9-*hSyn1*-DIO-$hM_3D(G_q)$-mCherry; Addgene, 44362) under the human *synapsin-1* promoter in Cre-positive mice. For validation of L5 neuron or interneuron activation in vivo (Fig. 1J, 5D), two viruses (Cre-dependent GCaMP6f and DREADD-$hM_3D(G_q)$) were mixed at equal volumes and injected into the PFC of Cre-positive mice using neonatal injection technique, and following weeks of expression, L5 and interneuron activity was imaged before and ~20-30 minutes after CNO i.p. injection. In experiments where interneurons were activated and L5 pyramidal neurons were imaged (Fig. 5E), AAV1-*hSyn1*-DIO-$hM_3D(G_q)$-mCherry was mixed with AAV1-*hSyn1*-GCaMP6f, and AAVs were injected into interneuron-specific Cre-positive mice as a neonate. GCaMP6f expressing neurons in L5 confirmed based on cortical depth from pial surface.

SK2 overexpression and knockdown.

SK2 channel overexpression in cells that normally lack endogenous SK2 expression was accomplished with expression of Cre-depedent mKCNN2 under the human *synapsin-1* promoter in Cre-expressing cells or Cre-positive mice (AAV9-*hSyn1*-DIO-mKCNN2-2A-mCherry; Vector Biolabs; reference sequence: NM_001312905; titer: 8.5x 10^{12} GC/mL)(Fig. 7C-D). SK2 channel knockdown in vivo and in vitro was accomplished by expression of Cre-dependent mKCNN2-shRNAmir under the *CAG* promoter in Cre-expressing cells or Cre-positive mice (AAV9-*CAG*-DIO-GFP-mKCNN2-shRNAmir#1; Vector Biolabs; reference sequence: NM_080465; titer: 6.4x 10^{12} GC/mL) (Fig. 7C-E, fig. S15). Based on shRNAmir#1

(5'- GCT GTCCATGTGAACGTATAATTCCGTTTTGG CCAC TGACTGACGGAATTATGTTCACATGGA CAG-3') screening, shRNAmir#1 yields 83% knockdown of mRNA (communication from Vector Biolabs). We confirmed this knockdown efficacy in cultured cortical neurons by measuring SK2 immunofluorescence in cells with or without shRNAmir#1 expression (~68% reduction of SK2 immunofluorescence in GFP-mKCNN2-shRNAmir#1 expressing cells as compared to GFP-scramble shRNA). Immunostaining protocol stated below with culture protocol.

NR1 knockdown.
NMDA-receptor NR1 subunit knockdown in vivo and in vitro was accomplished by packaging GRIN1 siRNA oligos in AAV9 (Abmgood; Cat. No. 22671174; reference sequence: NM_008169) (Fig. 3C, E, fig. S8). A scrambled siRNA AAV was used in parallel for control (Abmgood, 01509). Based on target sequences (Target a - 7 ACCATGCACCTGCTGACATTCGCCCTGCT, Target b - 969 GGTGCTGATGTCTTCCAAGTATGCAGATG, Target c - 1507 GGAGAGCTGCTCAGTGGTCAAGCAGACAT, Target d - 2591 ATAGAAAGAGTGGTAGAGCAGAGCCCGAC) siRNA oligos expression should produce a 70% knockdown of mRNA (communication from Abmgood). We confirmed this knockdown efficacy in cultured cortical neurons by measuring NR1 immunofluorescence in cells with siRNA to GRIN1 as compared to scrambled siRNA control (~50% reduction of NR1 expression) (fig. S8).

Chronic stress exposure
Chronic Corticosterone (CORT).
Mice were exposed to CORT in the drinking water for 21 days *(1, 2)*. CORT (Sigma-Aldrich, 27840) was dissolved in limiting amounts of 100% ethanol and mixed with animal facility-provided drinking water to a final concentration of 0.1 mg/ml CORT and 1% ethanol.

Chronic aggressor interactions (CAI).
Male C57BL/6 mice were chronically stressed with a screened aggressor male CD-1 mouse (Charles River Laboratories, <4 months of age) for 10 min daily for a total of 10 days in CD-1's home cage (fig. S1) *(3)*. CD1 mice are housed singly throughout (exception was during pairing with C57BL/6 mice). To determine an aggressive CD-1 mouse prior to chronic stress, we placed screener C57BL/6 mice (different from stressed cohort) directly into the home cage of the aggressor for 180 s with the aggressor present. During three 180 s screening sessions, once daily, the CD-1 mouse had to attack in at least two consecutive sessions, with a latency to initial aggression < 60 s. CD-1 mice that did not meet this criterion were not used. Our control group had normal drinking water and received gentle handling for ~15 minutes per day over 10 days prior to imaging.

Surgical preparation before in vivo imaging
In preparation for imaging, mice underwent a surgical procedure to attach a head holder mount and create an imaging window for two-photon microscopy. In brief, mice were anesthetized with a mixture of 100% oxygen at 2 L min−1 and 1-4% isoflurane. A heating pad was used to maintain the animal's body temperature at approximately 37 °C. The mouse's head was shaved, and its skull surface was exposed with a midline scalp incision. The periosteal tissue over the skull surface was removed without damaging the temporal and occipital muscles. A head holder consisting of two parallel metal bars was attached to the animal's skull. In Cre-positive mice injected with AAV, <1% of mice were negative for GCaMP/DREADD-mCherry fluorescence, suggesting that genotyping error or off-target injection was a rare event. If mice were negative for expression, mice were euthanized and not used. In positive mice, a small skull region (~2-4 mm in diameter) located over interfrontal suture was removed (or parietal bone for S1), and a round glass coverslip (approximately the same size as the bone being removed) was affixed to the skull with Loctite 495 followed by dental acrylic cement. This window enabled imaging of PFC (+0.5–1.0 mm anterior of bregma and 0.3–0.5 mm lateral to midline), M2 (+1.5-2.00 mm, +0.5-0.8 mm) or S1 (−0.1 mm, +2.0 mm).

Upon recovering from surgical anesthesia, mice with head mounts were habituated daily (two sessions of 30 minutes with 15-minute break) starting on postoperative day 1 in a custom-built body support to minimize potential stress effects of head restraining and imaging. No obvious distress was observed in habituated animals during imaging experiments. Mice tolerated surgery and stress related to the perioperative period as indicated by a 0–10% drop in weight. Imaging experiments were started on postoperative day 2-3 after window implantation.

Two-photon calcium imaging.
On the day of imaging, awake mice were positioned in the custom head holder device under the two-photon microscope. In vivo two-photon imaging was performed with an Olympus DIY RS two-photon system (tuned to 910-920 nm) equipped with a Coherent Discovery NX laser. We minimized movement associated image artifact by head (secured metal head bars) and body (with a plastic sleeve) restraint on the imaging platform. Mice were head-restrained and imaged for <1.5-2 hour in total, imaging across several regions in L2/3 or L5. Mice received one dose of N_2O (only exception was in Fig. 3 where ketamine was given) because of the potential interference of potentially N_2O-induced activity dependent plasticity. Calcium imaging was performed before and after 15-20 min of N_2O inhalation to increase the likelihood that the recordings were taken under a steady state concentration. Multiple imaging planes were taken across the cortical mantle with a typical acquisition of 3-4 planes in a given cortical layer after this 20-minute mark of inhalation. In Fig. 2, where the same mice were re-imaged hours later, the mice were placed back in their home cage with unlimited access to food and water. Pyramidal neurons and interneurons in cortical regions were randomly chosen and recorded for 2-minute sessions under awake conditions. Mice received N_2O (25, 50, 75 %; Airgas) mixed with O_2 (blended by Matrx MDS VMC anesthesia machine) or pure O_2 (100%) via nose cone under the two-photon microscope, and the same cortical regions were reimaged based on blood vessel maps. Exact N_2O concentration delivered post blending was monitored by a clinical Philips gas monitoring system (IntelliVue G5-M1019A/MP70; Medical grade device serviced by Penn Clinical Engineering) (Fig. 1A). All experiments were performed using a ×20 Olympus objective (XLUMPLFLN; 1.00 NA, 2.0 mm working distance) immersed in aCSF, with ×2-6 digital zoom. Images were acquired at a frame rate of 2-4 Hz (2-µs pixel dwell time). Image acquisition was performed using Olympus Fluoview software and analyzed post hoc using ImageJ software version 2.1.0.

Two-photon laser cutting of L5 tuft dendrites.
In Fig. 4 and fig. S9, dendrites expressing GCaMP6/tdTomato were cut by parking the two-photon laser beam on a small ROI that spanned the diameter of the dendrite for 5 s (tuned to ~890 nm and power was increased gradually until a sudden increase in fluorescence intensity was observed) *(4)*. After laser cut, a physical break could be observed between the two segments of dendrite. In the control experiment, the laser beam was parked ~30 µm away from the branch of interest without damaging it.

Systemic and local drug delivery.
Drugs delivered systemically were via a single i.p. injection: CNO 3 mg/kg (Sigma-Aldrich, C0832; solution of CNO in saline 0.3 mg/mL), ketamine 10 mg/kg or 100 µM (Sigma-Aldrich, 1356009), fluoxetine 10 mg/kg (Cayman, 14418), and naloxone 5 mg/kg (Cayman, 15594). In fig. S12, mice were coadministered N_2O with isoflurane (Baxter, 0.2 or 0.6%). Imaging was performed after 15 minutes of administration to ensure a steady state concentration in the animal.

Drugs of various concentrations and low injectate volumes (~1 µL) were delivered locally, MK801 at 10-100 µM (Sigma-Aldrich, M107); D-APV at 100 µM (Tocris, 0106); CNQX at 100 µM (Sigma-Aldrich, 115066-14-3); Apamin at 100 µM (Tocris, 1652) ; NS8593 at 100 µM (Tocris, 4597); TTX at 1 nM (Tocris, 1069); riluzone 10 µM (Cayman, 35833); Cadmium at 50 µM (Sigma-Aldrich, 265330); Dantrolene at 500 µM (Cayman, 14326); Xestospongin C at 500 µM (Cayman, 64950), CyPPA at 100 µM

(Cayman, 15614), muscimol at 10 μM (Sigma, 5060440001) via pressure application with a Picospritzer (20 p.s.i., 50 ms per pulse, 1 Hz, 5–10 pulses) to the surface of the PFC after removing a small bone flap (~200 μm in diameter) adjacent to the imaging window. The bone flap for drug delivery was made during head holder mounting and covered with a silicone elastomer such that it could be easily removed at the time of imaging. In some experiments, drugs were injected with Rhodamine 6G to measure the extent of spread within cortical tissue (Fig. 3A). As a control, we applied aCSF after removing the bone flap.

Cortical Cell culture

Mouse cortical neurons were prepared by Penn Medicine Translational Neuroscience Center (Neurons R US) and plated at a low density in a similar manner to our previous report *(5)*. Culture medium contained 500 mL of MEM (Invitrogen), 5% FBS (HyClone, Logan, UT), 10 mL of B-27 supplement (Invitrogen), 100 mg of NaHCO3, 20 mM D-glucose, 0.5 mM L-glutamine, and 25 units/ml penicillin/streptomycin. Neurons were maintained at 37 °C in a 5% CO_2-humidified incubator. AAV infection of GCaMP6f or shRNA/siRNA was performed on day 2 (2 days *in vitro* or DIV). Two-photon imaging of cultured neurons was performed on 7-9 DIV in a temperature-controlled chamber where neurons were recorded under normal bath solution followed by local application of glutamate 100 μM (Sigma-Aldrich, G1251) or bubbled N_2O bath solution (N_2O 50% mixed with O_2). For immunostaining of SK2 or NR1, cultured neurons infected with shRNA or siRNA respectively were rinsed with PBS twice and fixed for 15 min in a solution of 4% paraformaldehyde, pH 7.4. Coverslips were then rinsed three times in PBS. Cover slips were permeabilized for 1 hour at room temperature with blocking buffer (10% NGS, 0.5% Triton X in 0.1M PB). Primary antibodies were diluted in the blocking buffer and set to incubate overnight at 4 °C. SK2 was immunostained with rabbit monoclonal antibody (1:200; Boster Biological Technology, A05055). NR1 was identified with a NMDA-receptor 1 mouse monoclonal antibody (1:100; Fisher Scientific, 30-050-0). The next day, coverslips were rinsed three times in 0.1 M PBS for 10 min. Secondaries anti-mouse Cy3 or anti-rabbit Cy3 (Jackson ImmunoResearch) were diluted in blocking buffer and the coverslips were incubated for 2 hours at room temperature. Cover slips were rinsed four times in 0.1M PBS for 10 min and mounted with Vectashield (Vector Laboratories) on glass slides.

In vitro L5 recordings of mAHPs

Wild-type male mice aged 4-8 weeks were used for electrophysiological studies. Coronal brain slices (300 μm thick) were prepared as described previously*(6)*. Slices were perfused (2 ml/min) with oxygenated, artificial cerebrospinal fluid (aCSF) containing (in mM): 125 NaCl, 25 glucose, 25 $NaHCO_3$, 2.5 KCl, 1.25 NaH_2PO_4, 2 $CaCl_2$, and 1 $MgCl_2$; 310 mOsM; pH 7.3-7.4), equilibrated with 95% O_2/5% CO_2. Layer 5 pyramidal neurons were identified by location and morphology (large cell body with prominent apical dendrite). Whole-cell recordings were performed using borosilicate glass pipettes (World Precision Instruments, 3-6 MΩ) filled with K-$MeSO_4$ internal solution containing (in mM): 130.5 K-$MeSO_4$, 10 KCl, 7.5 NaCl, 2 $MgCl_2$, 10 HEPES, 0.1 EGTA, 2 MgATP, and 0.2 NaGTP; 290 mOsM; pH 7.3-7.4). mAHPs were recorded in current-clamp mode. Baseline recordings commenced 5 min after break-in to ensure stabilization. For N_2O experiments, aCSF containing 30% N_2O was prepared by mixing aCSF equilibrated with 95% N_2O/5% CO_2 and aCSF equilibrated with 95% O_2/5% CO_2. This solution was perfused for 5 minutes before recordings. Amplitude of mAHP was measured using Clampfit (Molecular Devices, San Jose, CA). Graphs and statistical analysis were performed in GraphPad Prism (Dotmatics, Boston, MA).

Data analysis

Behavior tests.

Behavior testing was conducted 30-60 min after post-N_2O therapy. In tail suspension test (TST; Fig. 1B, fig. S1) *(7)*, mice were suspended from the edge of a table (60 cm high) by an adhesive tape placed approximately 1 cm from the tip of the tail. In TST, mice transition between complex escape movements, such as swinging and curling, mixed with periods of immobility over 6 minutes of video recording (first

two minutes are discarded because of increased activity when placed in tail suspension). Videos and measurements were made using ANYMaze software (Stoelting).

In the elevated plus maze (EPM) *(8)*, mice were placed in the center of the maze, which consisted of two open arms without walls and two closed arms with walls. The time spent over 10 min recording period in each arm of the maze was recorded using a camera suspended on scaffold and analyzed using ANYMaze. The maze was cleaned with an alcohol solution between trials.

In the sucrose preference test *(9)*, mice were individually housed and given two bottles of tap water for 2 days. On day 3, once water intake was stable, one bottle was swapped for 0.6% sucrose water and volume intake was recorded for the next 12 hr. The position of the sucrose bottle was randomly shuffled every 2 hours. Preference for sucrose was calculated as the volume of sucrose consumed minus the volume of water, divided by the total intake volume, yielding a ratio from -1 to +1. Positive score indicates a sucrose preference, negative score a water preference, and a zero score suggests no preference.

To determine the effect of 50% N_2O on animal behavior in the absence of head-restraining we created a closed chamber (12 x 7 x 8 inches; ~11 liters) with a port to receive blended N_2O/O_2 (fig. S2). Spontaneous movement was first tracked in a pure O_2 environment for 5 min. Following this period, the chamber was transitioned to N_2O 50% (2L/min) for a period of 15 min to enable equilibrium prior to another 5 min recording. Total distance, average speed, and max speed over 5 min period was recorded by ANYMaze during both conditions.

EEG recordings.
Epidural EEG leads were placed in M2 and RS cortex (0.3 mm and 1.6 mm posterior to bregma, 0.65 mm lateral to bregma). In fig. S5, EEG signals were recorded over wakefulness and increasing N_2O (25, 50, 75%) at 1,000 Hz using a 32-channel headstage (Intan Technologies) using methodology previously described *(10, 11)*. Each step was recorded for 30 minutes, where the final 10 minutes were used for subsequent analysis to ensure steady state. Differential biopotentials were processed and analyzed in MATLAB (2020b, Mathworks) with the Signal Processing and Statistics and Machine Learning toolboxes and custom code to compute power spectra under baseline wakefulness and N_2O conditions using a multi-taper method (15 tapers, 5-second non-overlapping windows)*(12)*. Error estimation was computed using bootstrap resampling with replacement (1,000 bootstraps, across windows) to produce 95% confidence intervals. Deviations from baseline were computed by subtracting the mean baseline power spectrum from each spectral window after injection. EEG was bandpass filtered (6th order Butterworth) from 0.5 Hz to 100 Hz before spectral estimation and normalized by total power for each spectral window.

Two-photon in vivo recordings.
During recordings, motion-related artifacts were typically less than 2 μm. Vertical movements were infrequent and minimized by two metal bars attached to the animal's skull (described above) and a custom-built body support. All time-lapse images from each individual field of view were motion-corrected and referenced to a single template frame using cross-correlation image alignment (TurboReg plugin for ImageJ version 2.1.0). ROIs corresponding to visually identifiable somas (pyramidal cells and interneurons) were selected manually from the field of view. Imaging planes were acquired from L2/3 and L5, corresponding to cells positioned ~150–350 μm and ~500–750 μm from the pial surface respectively. Note that our neonatal injections produced sparse to moderate labelling of GCaMP6 throughout all layers in PFC. As one can see in Fig. 1, 5–20 neurons per L2/3 or L5 imaging region was common. A typical experiment would include 3–4 (randomly chosen) imaging regions per animal, yielding ~20–40 cells per animal. Somas that could be identified in all imaging sessions were included in the dataset.

mRNA expression analysis from Allen Brain Cell Type specific dataset.

We queried the 10x scRNAseq whole brain dataset from Allan Brain Cell Atlas *(13)* to identify gene expression levels of candidate channels and receptors (Kcnq2, Kcna1, Hcn1, Scn1a, Scn1b, Scn2a, Scn3a, Cacna1c, Ryr1, Itpr3, Oprm1, Grin1, Kcnn1, Kcnn2, Kcnn3, Grm1) across select neuronal cell types (L2/3, L5 IT, L5 ET, VIP, SST, PV). We limited our search to include feature matrix labels from cortical regions only and cell types to be restricted to cortex as well. A total of 109,503 individual cells were included in this analysis (L2/3 = 49,196 cells, L5 IT = 19,905 cells, L5 ET = 5,990 cells, VIP = 11,857 cells, SST = 13,845 cells, VIP = 9,070 cells). Distributions of gene expression are shown as log2(CPM +1) as violin plots, where black line denotes means, red line denotes medians. CPM = counts per million (transcript reads). Using this screen, we identified the SK2 channel, encoded by the Kcnn2 gene, to be specifically enriched in Layer 5 ET (extratelencephalic) and VIP neurons as compared to other cell types (L2/3, L5 IT, SST, PV) (fig. S14).

Analysis of calcium signals.
In this study, we used GCaMP6f, an indirect reporter of neuronal spiking activity. All the pixels inside the ROI were averaged to obtain a fluorescence trace for each ROI. Background fluorescence was calculated as the average pixel value per frame from a region without GCaMP expression (blood vessel) and subtracted from the time-series fluorescence traces. The baseline (F_0) of the fluorescence trace was estimated by the average of inactive portions of the traces (~2 seconds). We did not smooth the raw fluorescence trace (raw traces are presented throughout the manuscript in each figure). The $\Delta F/F_0$ (%) was calculated as $\Delta F/F_0 = (F - F_0) / F_0 \times 100$. Representative traces from a given cortical region are selected at random.

GCaMP6f can produce large fluorescence transients (~20% $\Delta F/F$) even in response to single action potentials, and individual spikes within a burst result in stepwise fluorescence increases *(14)*. However, when neuronal firing rates are high, it becomes difficult to resolve the number of action potentials owing to the long decay time constant of GCaMP6 fluorescence. We found that there was a diversity in calcium traces of pyramidal cells in wakefulness and under N_2O, which likely reflects burst and nonburst firing of L5 neurons. Although it is difficult to report firing rates based on calcium responses within individual cells, several studies using two-photon imaging and patch-clamp electrophysiology have found a significant correlation between calcium signals and action potential generation in neuronal cell types *in vivo*. To compare neuronal activity among different cells, we performed an integrated measurement of a cell's output activity over 2 min recording, termed area under the curve (AUC, %), as well as measuring peak fluorescence signal.

The effect of either N_2O or ketamine was defined as the difference in L5 $\Delta F/F_0$ in drug-induced state and wakefulness. In Fig. 3F where a scatter plot of calcium activity of individual L5 neurons are shown, we compute the Pearson correlation coefficient. The *P* value associated with the correlation coefficient was computed by transforming the correlation coefficient to an *F*-statistic having $n-1$ and $n-2$ degrees of freedom, where n is the number of neurons. Negative correlation coefficients in this case mean that N_2O and ketamine activated neurons differently.

SK2 channel molecular dynamics simulations
System setup. A homology model for human SK2 was constructed using SWISSMODEL *(15)* with open-state, calmodulin-bound human SK4 channel (PDB 6CNN) as a template structure *(16)*. The template structure has calcium and calmodulin bound, yielding an open channel state. SK2 sequences are 98.8% identical between human and mouse. The resulting highest-scoring homology model, with calmodulin in the same bound position and conformation as in the SK4 structure, was embedded in a POPC:cholesterol 3:1 lipid membrane, using CHARMM-GUI *(17, 18)*. The channel was oriented with the major pore axis parallel to the simulation box z-axis.

Simulations. A single N_2O molecule, using previously described molecular mechanics parameters *(19)*, was placed in the SK2 channel selectivity filter. A volume restraint, upon which a restoring force would be imposed upon migration greater than 8 Å away from the initial position, was placed on the N_2O molecule. NAMD 3 was used for all simulations *(20)*. Minimization and equilibration followed. Production simulation in the isothermic-isobaric ensemble with Langevin dynamics (2 fs timestep, Particle Mesh Ewald used for long-range electrostatics with 10 Å switching distance and 12 Å cutoff) for 20 ns followed. As the ligand remained in the pocket without migration further than 8 Å, the volume restraint did no work. To generate a potential of mean force (PMF) profile of the movement of N_2O along the pore axis in the immediate region of the selectivity filter, we conducted adaptive biasing force simulations *(21)*. The position of the N_2O molecule along the pore axis was measured using the Colvars module *(19, 22)*, as the z-component of the distance between the center of gravity of the N_2O and the averaged center of mass of the C-alpha atoms of the Tyr361 residues (in the selectivity filter) in each of the 4 monomers comprising SK2. Data was collected in 0.1 Å bins. In each bin, 500 steps were discarded prior to collecting ABF data. Each ABF calculation spanned 6 Å along the pore axis. A total of 15 replicate calculations over a total of 135 ns were run.

General statistical analysis

Animals were randomly assigned to experimental groups. No statistical methods were used to pre-determine sample sizes, but our sample sizes for in vivo imaging and behavior studies are similar to those reported in our previous publications and others *(4, 23–26)*. The interventions were not blinded as nearly all experiments were carried out and analyzed by J.C. We tested the data for normality using the Shapiro-Wilk test and performed parametric statistical tests. Two-way ANOVA was used in Fig. 1B-D, K, 3C, E. If normality was not present, we performed nonparametic tests, including Wilcoxon rank sum test (or t test) to compare two groups and Kruskal-Wallis (or one-way ANOVA) to compare more than two groups. Kruskal-Wallis (or One-way ANOVA) tests were followed by Dunn's multiple comparisons test for multiple comparisons. Mean ± s.e.m. was used to report statistics unless otherwise indicated. The statistical test used and the definition of *n* for each analysis are listed in the text or figure legends. Tests were computed in GraphPad Prism version 9.3.1. EEG analysis and mRNA expression plots were performed in MATLAB (2023a) with custom scripts. Criteria for animal exclusion was pre-established: mice were excluded if the injected virus did not express. Exact *P* values are reported in figures and legends.

References:

1. R. N. Moda-Sava, M. H. Murdock, P. K. Parekh, R. N. Fetcho, B. S. Huang, T. N. Huynh, J. Witztum, D. C. Shaver, D. L. Rosenthal, E. J. Alway, K. Lopez, Y. Meng, L. Nellissen, L. Grosenick, T. A. Milner, K. Deisseroth, H. Bito, H. Kasai, C. Liston, Sustained rescue of prefrontal circuit dysfunction by antidepressant-induced spine formation. *Science* **364** (2019), doi:10.1126/science.aat8078.
2. S. A. Johnson, N. M. Fournier, L. E. Kalynchuk, Effect of different doses of corticosterone on depression-like behavior and HPA axis responses to a novel stressor. *Behav. Brain Res.* **168**, 280–288 (2006).
3. S. A. Golden, H. E. Covington 3rd, O. Berton, S. J. Russo, A standardized protocol for repeated social defeat stress in mice. *Nat. Protoc.* **6**, 1183–1191 (2011).
4. J. Cichon, W.-B. Gan, Branch-specific dendritic Ca2+ spikes cause persistent synaptic plasticity. *Nature* **520**, 180–185 (2015).
5. J. Cichon, C. Sun, B. Chen, M. Jiang, X. A. Chen, Y. Sun, Y. Wang, G. Chen, Cofilin aggregation blocks intracellular trafficking and induces synaptic loss in hippocampal neurons. *J. Biol. Chem.* **287**, 3919–3929 (2012).
6. X. Lu, P. Lambert, A. Benz, C. F. Zorumski, S. J. Mennerick, Allopregnanolone effects on inhibition in hippocampal parvalbumin interneurons. *eNeuro* **10**, ENEURO.0392-22.2023 (2023).

7. J. F. Cryan, C. Mombereau, A. Vassout, The tail suspension test as a model for assessing antidepressant activity: review of pharmacological and genetic studies in mice. *Neurosci. Biobehav. Rev.* **29**, 571–625 (2005).
8. A. A. Walf, C. A. Frye, The use of the elevated plus maze as an assay of anxiety-related behavior in rodents. *Nat. Protoc.* **2**, 322–328 (2007).
9. M.-Y. Liu, C.-Y. Yin, L.-J. Zhu, X.-H. Zhu, C. Xu, C.-X. Luo, H. Chen, D.-Y. Zhu, Q.-G. Zhou, Sucrose preference test for measurement of stress-induced anhedonia in mice. *Nat. Protoc.* **13**, 1686–1698 (2018).
10. A. Z. Wasilczuk, A. Proekt, M. B. Kelz, A. R. McKinstry-Wu, High-density electroencephalographic acquisition in a rodent model using low-cost and open-source resources. *J. Vis. Exp.* (2016), doi:10.3791/54908.
11. J. H. Siegle, Open Ephys: an open-source, plugin-based platform for multichannel electrophysiology.
12. A. E. Hudson, D. P. Calderon, D. W. Pfaff, A. Proekt, Recovery of consciousness is mediated by a network of discrete metastable activity states. *Proc. Natl. Acad. Sci. U. S. A.* **111**, 9283–9288 (2014).
13. Z. Yao, C. T. J. van Velthoven, M. Kunst, M. Zhang, D. McMillen, C. Lee, W. Jung, J. Goldy, A. Abdelhak, P. Baker, E. Barkan, D. Bertagnolli, J. Campos, D. Carey, T. Casper, A. B. Chakka, R. Chakrabarty, S. Chavan, M. Chen, M. Clark, J. Close, K. Crichton, S. Daniel, T. Dolbeare, L. Ellingwood, J. Gee, A. Glandon, J. Gloe, J. Gould, J. Gray, N. Guilford, J. Guzman, D. Hirschstein, W. Ho, K. Jin, M. Kroll, K. Lathia, A. Leon, B. Long, Z. Maltzer, N. Martin, R. McCue, E. Meyerdierks, T. N. Nguyen, T. Pham, C. Rimorin, A. Ruiz, N. Shapovalova, C. Slaughterbeck, J. Sulc, M. Tieu, A. Torkelson, H. Tung, N. V. Cuevas, K. Wadhwani, K. Ward, B. Levi, C. Farrell, C. L. Thompson, S. Mufti, C. M. Pagan, L. Kruse, N. Dee, S. M. Sunkin, L. Esposito, M. J. Hawrylycz, J. Waters, L. Ng, K. A. Smith, B. Tasic, X. Zhuang, H. Zeng, A high-resolution transcriptomic and spatial atlas of cell types in the whole mouse brain*bioRxiv* (2023), doi:10.1101/2023.03.06.531121.
14. T.-W. Chen, T. J. Wardill, Y. Sun, S. R. Pulver, S. L. Renninger, A. Baohan, E. R. Schreiter, R. A. Kerr, M. B. Orger, V. Jayaraman, L. L. Looger, K. Svoboda, D. S. Kim, Ultrasensitive fluorescent proteins for imaging neuronal activity. *Nature* **499**, 295–300 (2013).
15. A. Waterhouse, M. Bertoni, S. Bienert, G. Studer, G. Tauriello, R. Gumienny, F. T. Heer, T. A. P. de Beer, C. Rempfer, L. Bordoli, R. Lepore, T. Schwede, SWISS-MODEL: homology modelling of protein structures and complexes. *Nucleic Acids Res.* **46**, W296–W303 (2018).
16. C.-H. Lee, R. MacKinnon, Activation mechanism of a human SK-calmodulin channel complex elucidated by cryo-EM structures. *Science* **360**, 508–513 (2018).
17. J. Lee, X. Cheng, J. M. Swails, M. S. Yeom, P. K. Eastman, J. A. Lemkul, S. Wei, J. Buckner, J. C. Jeong, Y. Qi, S. Jo, V. S. Pande, D. A. Case, C. L. Brooks 3rd, A. D. MacKerell Jr, J. B. Klauda, W. Im, CHARMM-GUI Input Generator for NAMD, GROMACS, AMBER, OpenMM, and CHARMM/OpenMM Simulations Using the CHARMM36 Additive Force Field. *J. Chem. Theory Comput.* **12**, 405–413 (2016).
18. S. Jo, T. Kim, V. G. Iyer, W. Im, CHARMM-GUI: a web-based graphical user interface for CHARMM. *J. Comput. Chem.* **29**, 1859–1865 (2008).
19. K. Töpfer, D. Koner, S. Erramilli, L. D. Ziegler, M. Meuwly, Molecular-level understanding of the rovibrational spectra of NO in gaseous, supercritical, and liquid SF and Xe. *J. Chem. Phys.* **158**, 144302 (2023).
20. J. C. Phillips, R. Braun, W. Wang, J. Gumbart, E. Tajkhorshid, E. Villa, C. Chipot, R. D. Skeel, L. Kalé, K. Schulten, Scalable molecular dynamics with NAMD. *J. Comput. Chem.* **26**, 1781–1802 (2005).
21. E. Darve, A. Pohorille, Calculating free energies using average force. *J. Chem. Phys.* **115**, 9169–9183 (2001).
22. G. Fiorin, M. L. Klein, J. Hénin, Using collective variables to drive molecular dynamics simulations. *Mol. Phys.* **111**, 3345–3362 (2013).
23. J. Cichon, A. Z. Wasilczuk, L. L. Looger, D. Contreras, M. B. Kelz, A. Proekt, Ketamine triggers a switch in excitatory neuronal activity across neocortex. *Nat. Neurosci.* **26**, 39–52 (2023).

24. J. Cichon, T. J. J. Blanck, W.-B. Gan, G. Yang, Activation of cortical somatostatin interneurons prevents the development of neuropathic pain. *Nat. Neurosci.* **20**, 1122–1132 (2017).
25. A. Adler, R. Zhao, M. E. Shin, R. Yasuda, W.-B. Gan, Somatostatin-expressing interneurons enable and maintain learning-dependent sequential activation of pyramidal neurons. *Neuron* **102**, 202-216.e7 (2019).
26. G. Yang, C. S. W. Lai, J. Cichon, L. Ma, W. Li, W.-B. Gan, Sleep promotes branch-specific formation of dendritic spines after learning. *Science* **344**, 1173–1178 (2014).

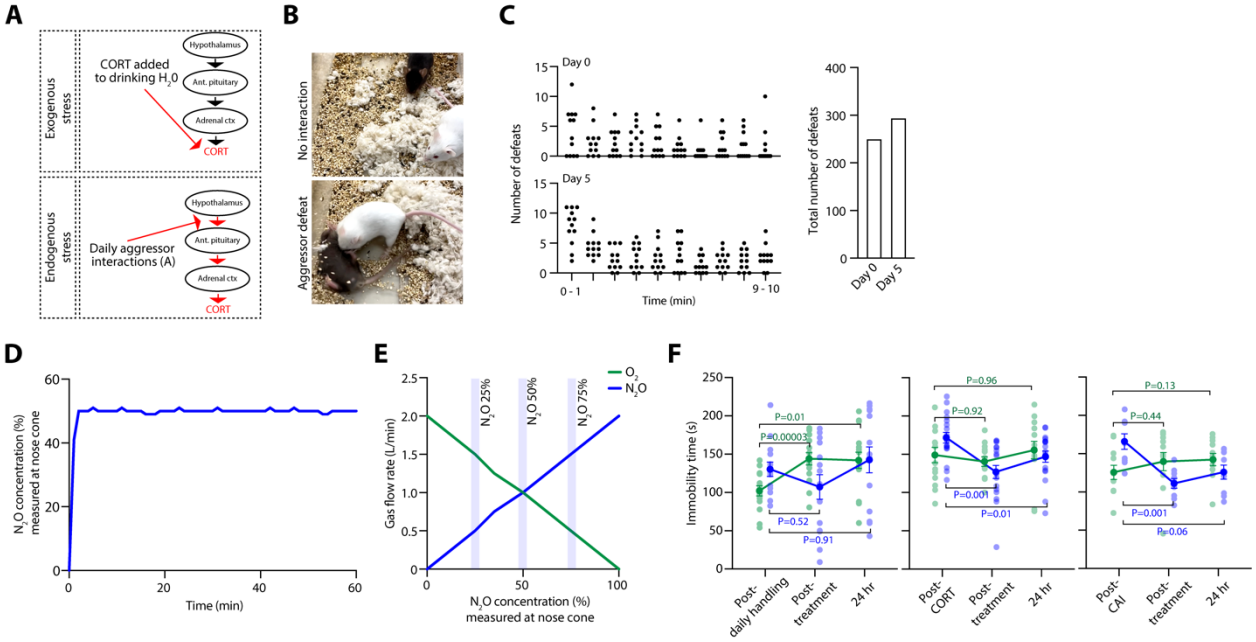

Supplemental Fig. 1. N_2O exposure induces a sustained antidepressant-like response in chronically stressed mice but not wild-type mice.

A, Left, schematic showing two different methods for driving the hypothalamus-pituitary-adrenal axis. Corticosterone added to drinking water for 21 days represents the exogenous manipulation (top) whereas male C57/BL6 mice exposed to daily interactions (10 min/day) with a male CD-1 (screened for aggression) mouse for 10 days is referred to as the endogenous manipulation (bottom).

B, Representative defeat experienced by C57BL/6 mouse exposed to screened aggressor mouse. C57BL/6 mouse is often forced on its backside (lower image).

C, Left, number of defeats over a 10 min period on first day of pairing (day 0) and day 5 experienced by 12 C57BL/6 mice. Right, total number of defeats experienced by same cohort on day 0 and day 5.

D, N_2O concentration sampled by Philips clinical gas monitoring system at nose cone during two-photon recording.

E, Blended gas mixtures for different N_2O concentrations, i.e. 25%, 50%, and 75%, while total output remains at 2 liters/min.

F, Serial tail suspension measurements were performed in control (left; O_2, n = 15; N_2O, n = 7), CORT (middle; O_2, n = 13; N_2O, n = 18), and CAI (right; O_2, n = 11; N_2O, n = 9) mice before and after oxygen (O_2) or N_2O exposure at 1 and 24 hr. Chronically stressed mice exposed to N_2O, but not O_2, for 1 hr developed a sustained decrease in immobility at 1 hr post treatment that persisted up to 24 hr (two-way

ANOVA time x treatment: control, $F_{(1.4, 38)} = 4.1$, $P = 0.004$; CORT, $F_{(1.8, 53)} = 5.8$, $P = 0.03$; CAI, $F_{(1.8, 33)} = 4.6$, $P = 0.00002$ with post hoc Sidak's multiple comparisons shown in each panel.

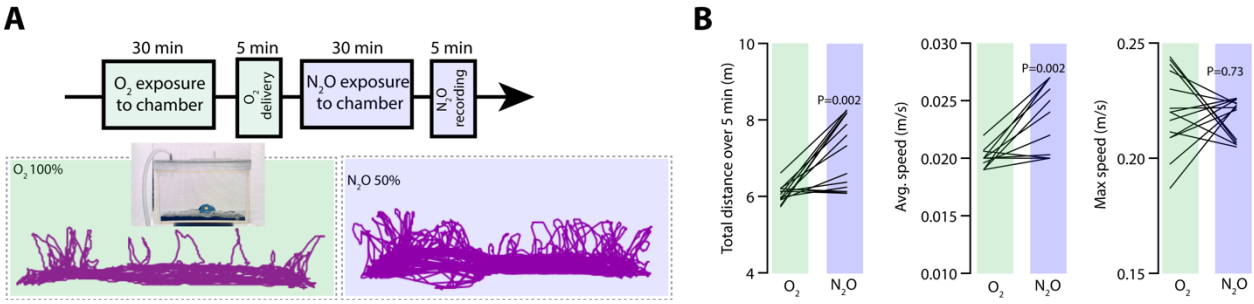

Supplemental Fig. 2. N_2O exposure at 50% increases animal movement and exploration.
A, The effect of O_2 (100%, top) or N_2O (50%, bottom) on animal's spontaneous movement (not head-fixed; $n = 15$). A representative 5 min tracing (produced by AnyMaze) of an individual animal's movement across closed chamber after 30 min of gas exposure (to ensure equilibrium). Horizontal lines capture movement across chamber whereas vertical lines note exploratory movements. N_2O increased both the horizontal and vertical movements.
B, Total distance, average speed, and max speed over 5 min period of all mice tested in O_2 and then N_2O. N_2O significantly increased the total distance (Wilcoxon matched-pairs signed rank test, $P = 0.002$) and average speed (Wilcoxon matched-pairs signed rank test, $P = 0.002$), but not max speed (Wilcoxon matched-pairs signed rank test, $P = 0.73$).

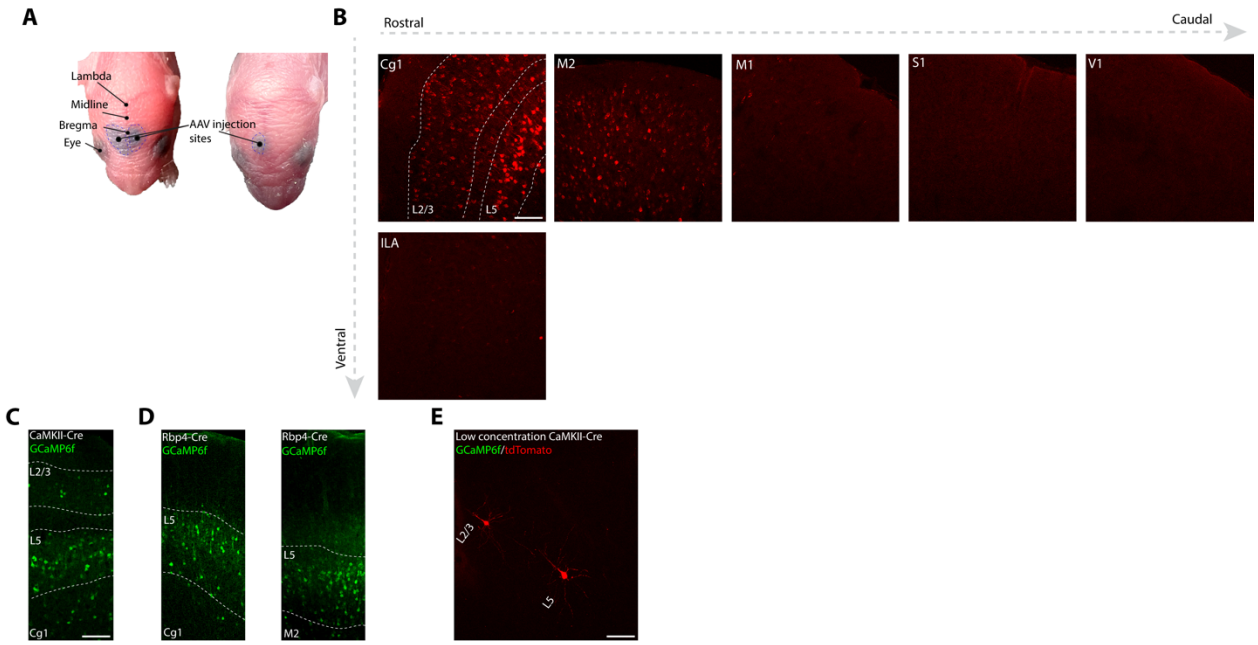

Supplemental Fig. 3. Postnatal adeno-associated virus injection strategy enables genetically encoded sensor targeting to prefrontal cortical regions.

A, Photograph of postnatal day 1 pup injected with cocktail of AAV and dye in a bilateral (left) or unilateral (right) approach. One postnatal day 1-2, landmarks (hemispheres, lambda, bregma, eyes, etc.) can be visible which aids in successful injection and AAV targeting.

B, Postnatal injection of AAVs harboring CaMKII-Cre and Cre-dependent tdTomato into medial prefrontal cortex (PFC). Coronal sections demonstrate the expression of tdTomato in layer 2/3 (L2/3) and layer 5 (L5) in Cg1 and M2 of PFC but not in neighboring areas (primary motor cortex (M1) or infralimbic cortex (ILA)) or in distant regions (primary somatosensory (S1) or visual cortices (V1)).

C, Coronal sections depicting AAV encoding CaMKII-Cre drove GCaMP6f expression in L2/3 and L5 of Cg1.

D, Transgenic Rbp4-Cre mice drove specific layer 5 in Cg1 (left) or M2 regions (right).

E, Diluted AAV-CaMKII-Cre produced sparse labelling of L2/3 and/or L5 neurons. Sparse labelling is critical to structure-function mapping of individual L5 neurons (Fig. 4). Scale bar, 100 μm for all images.

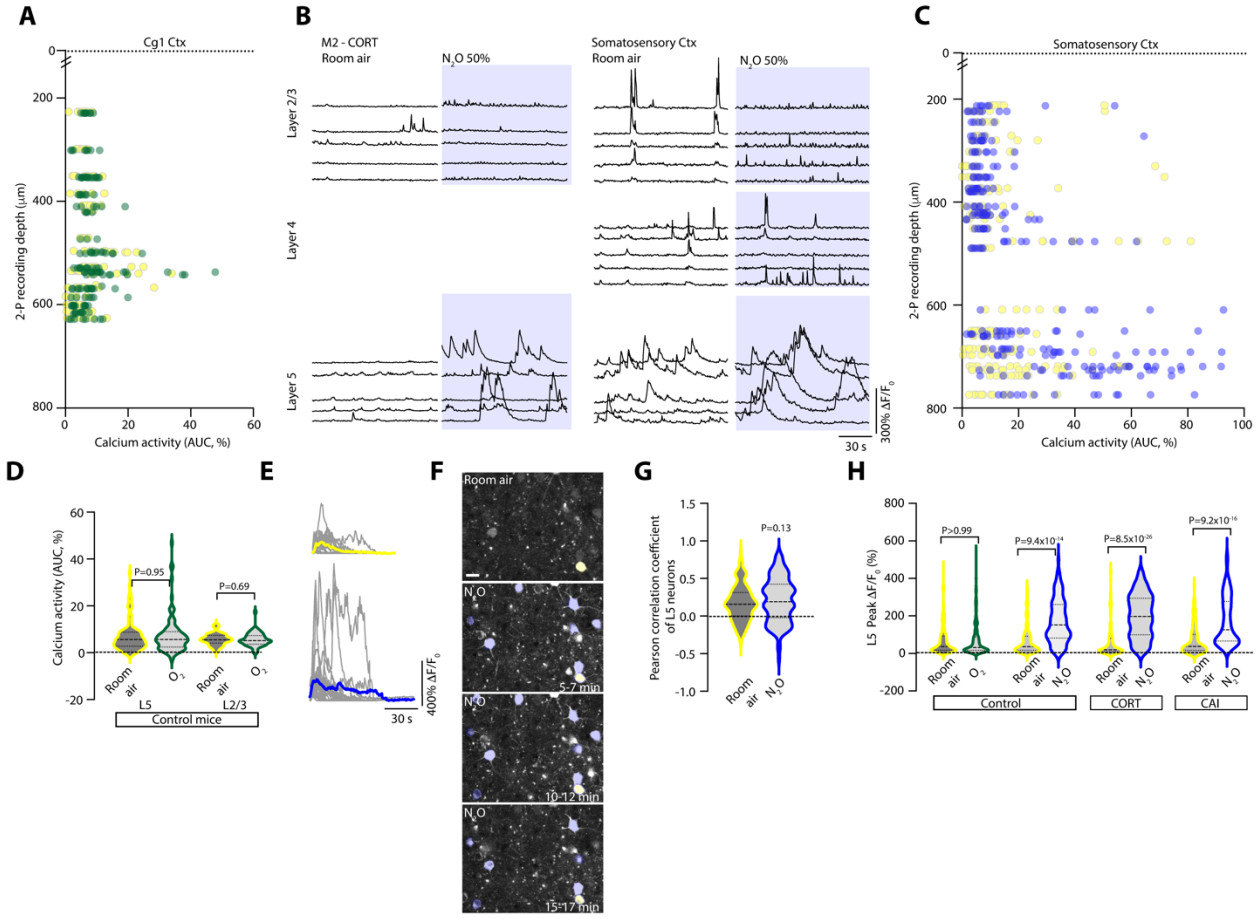

Supplemental Fig. 4. N_2O, but not oxygen therapy, recruits Layer 5 neuronal activity.
A, All neurons recorded in layer 2/3 (L2/3) or layer 5 (L5) under room air and O_2 therapy (100%) from across the Cg1 cortical column. Note the overlapping activity of excitatory neurons between wakefulness/room air (yellow) and O_2 (green).
B, Left, representative GCaMP6 traces of individual pyramidal neurons from L2/3 or L5 of M2 region under room air and N_2O inhalation in CORT-treated mouse. Right, representative GCaMP6 traces of individual pyramidal neurons spanning from L2/3 to L5 in the somatosensory cortex (S1) under room air and N_2O.
C, All neurons recorded from across the S1 cortical column. Note the N_2O-induced activation of L5 neurons a depth of >600 µm.
D, Average calcium response of L5 (n = 96) and L2/3 neurons (n = 56) under wakefulness/room air and O_2 therapy in control mice. O_2 fails to activate either cell type (Wilcoxon matched-pairs signed rank: L5, P = 0.95, L2/3, P = 0.69).
E, Individual transients from L5 neuron under room air (top) and N_2O (bottom). Note the sustained calcium elevation under N_2O condition.
F, Two-photon movies (2 min time-series) of L5 neurons collapsed into a single image over various time points into a N_2O inhalational event. L5 neurons are repetitively activated under N_2O (shaded blue). Scale bar, 20 µm.

G, Pearson correlation coefficient measurements between pairs of L5 neurons under room air and N_2O (n = 122; Wilcoxon matched-pairs signed rank, P = 0.13).

H, Peak $\Delta F/F_0$ of L5 neurons under room air (yellow) and N_2O (blue) in control and chronically stressed mice. N_2O induced a robust increase in peak signals across all conditions (Kruskal-Wallis (312): $P = 1.1 \times 10^{-63}$ followed by Dunn's multiple comparisons, WT O_2: $P > 0.99$; WT N_2O: $P = 9.4 \times 10^{-14}$; CORT N_2O: $P = 8.5 \times 10^{-26}$; CAI N_2O: $P = 9.2 \times 10^{-16}$).

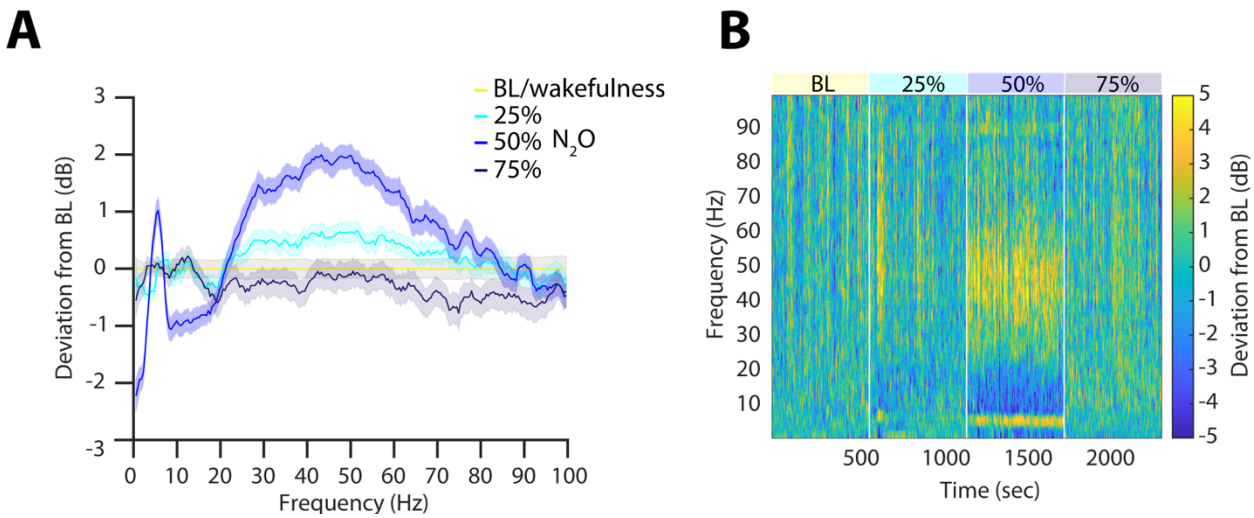

Supplemental Fig. 5. N_2O at 50% induces an activated electroencephalogram.
A, Differences in power across EEG frequencies induced by N_2O (25, 50, 75%) from its baseline measures recorded under room air conditions.
B, Power spectrogram across increasing N_2O concentrations. Note the increase in higher frequency oscillations with inhaled N_2O 50%.

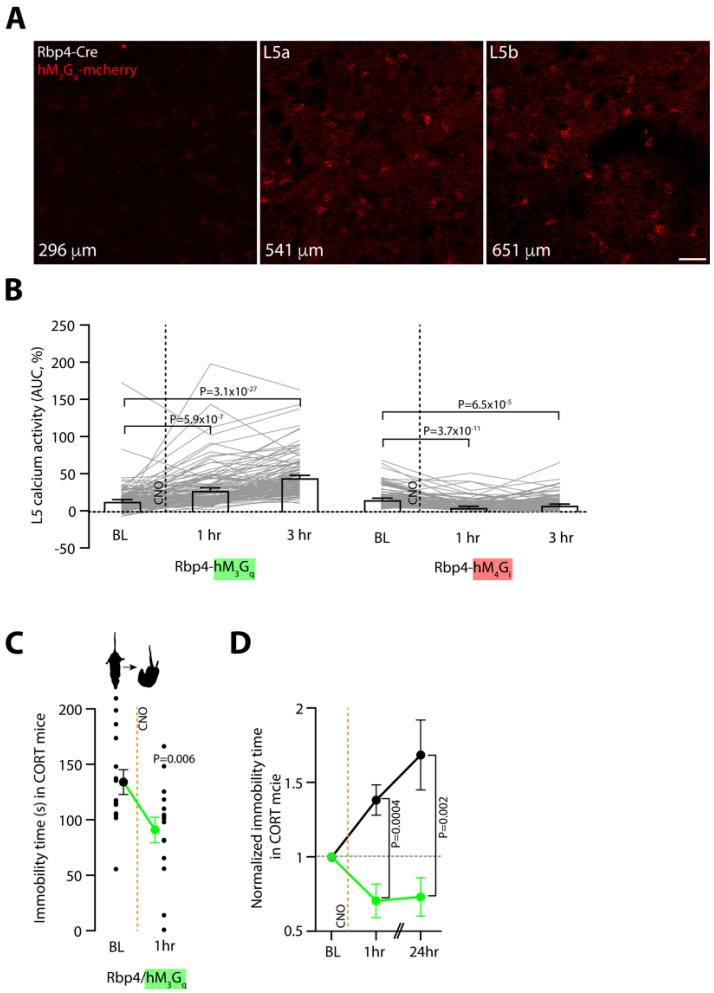

Supplemental Fig. 6. L5 neuronal expression of DREADD-hM$_3$G$_q$-mcherry and its activation drives persistent neuronal activity.

A, Two-photon images of hM$_3$G$_q$-mcherry expression in Rbp4-Cre mice. hM$_3$G$_q$-mcherry was expressed in L5a and L5b (right two images) but not layer 2/3 (left image). Scale bar, 20 µm.

B, Average calcium response of L5 neurons expressing either hM$_3$G$_q$-mcherry (left; n = 108 cells from 3 mice) or hM$_4$G$_i$-mcherry (right) before and after CNO injection. CNO-induced activation of L5-hM$_3$G$_q$ drove an increased activity state over hours (Kruskal-Wallis (118): $P = 2.0 \times 10^{-27}$ followed by Dunn's multiple comparisons, 1 hr: $P = 5.9 \times 10^{-7}$; 3 hr: $P = 3.1 \times 10^{-27}$). In contrast, L5-hM$_4$G$_i$ (right; n = 90 cells from 3 mice) activation induced a persistent hypoactivity over hours (Kruskal-Wallis (46): $P = 1.1 \times 10^{-10}$ followed by Dunn's multiple comparisons, 1hr: $P = 3.7 \times 10^{-11}$; 3hr: $P = 6.5 \times 10^{-5}$).

C, Immobility time during tail suspension in CORT treated Rbp4-Cre mice (n = 15) expressing hM$_3$G$_q$ bilaterally in PFC before and after CNO injection (Paired t-test (t = 3.3, df =14): $P = 0.006$).

D, Sustained decrease in immobility time during TST following a single injection of CNO in CORT treated Rbp4-Cre mice expressing hM3Gq bilaterally in PFC (n = 7) as opposed to Rbp4-Cre mice expressing tdTomato (n = 11; Mann Whitney rank sum test: 1 hr, $P = 0.0004$; 24 hr, $P = 0.002$).

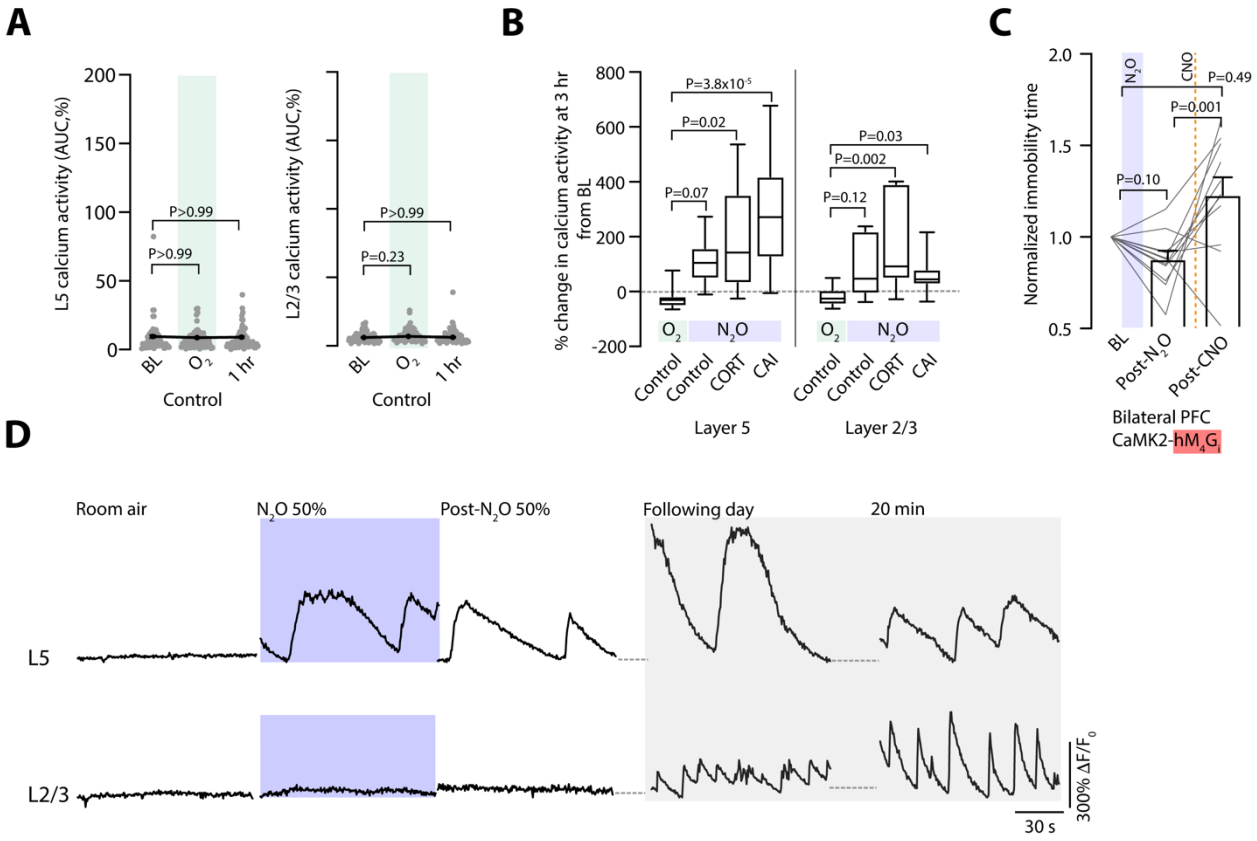

Supplemental Fig. 7. N_2O drives persistent L5 neuronal activity following exhalation.
A, Average calcium responses of L5 and L2/3 neurons under room air, O_2, and following O_2 therapy at 1 hr. O_2 failed to recruit either cell types following gas removal (WT L5 O_2, $n = 74$ cells from 3 mice, Kruskal-Wallis (0.07): $P = 0.96$; WT L2/3, $n = 99$ cells from 3 mice, Kruskal-Wallis (3): $P = 0.19$). Dunn's multiple comparisons shown in plot.
B, Percentage change in spontaneous activity at 3 hr time point from N_2O exposure normalized to its baseline recorded under room air conditions. At 3 hr timepoint, CORT ($n = 7$) and CAI ($n = 12$) mice show persistent L5 (Kruskal-Wallis (19.3): $P = 0.0002$ followed by Dunn's multiple comparisons, control, $P = 0.07$; CORT, $P = 0.02$; CAI, $P = 3.8 \times 10^{-5}$) and L2/3 (Kruskal-Wallis (12.9): $P = 0.004$ followed by Dunn's multiple comparisons, control, $P = 0.12$; CORT, $P = 0.002$; CAI, $P = 0.03$) activity as compared to control mice ($n = 10$) treated with O_2 or N_2O.
C, Immobility time of mice expressing CaMK2-hM_4G_i in PFC bilaterally ($n = 10$ mice) across N_2O exposure followed by CNO-induced inhibition of both L2/3 and L5 activity in this region. CNO-induced hM_4G_i activation promoted the reversal N_2O-induced behavioral effect (Kruskal-Wallis (13): $P = 0.002$ followed by Dunn's multiple comparisons, BL vs. Post N_2O: $P = 0.10$; Post N_2O vs. Post CNO: $P = 0.001$; BL vs. Post CNO: $P = 0.49$).
D, Representative traces from L5 and L2/3 cells that become activated during N_2O and at multiple timepoints following the N_2O exposure.

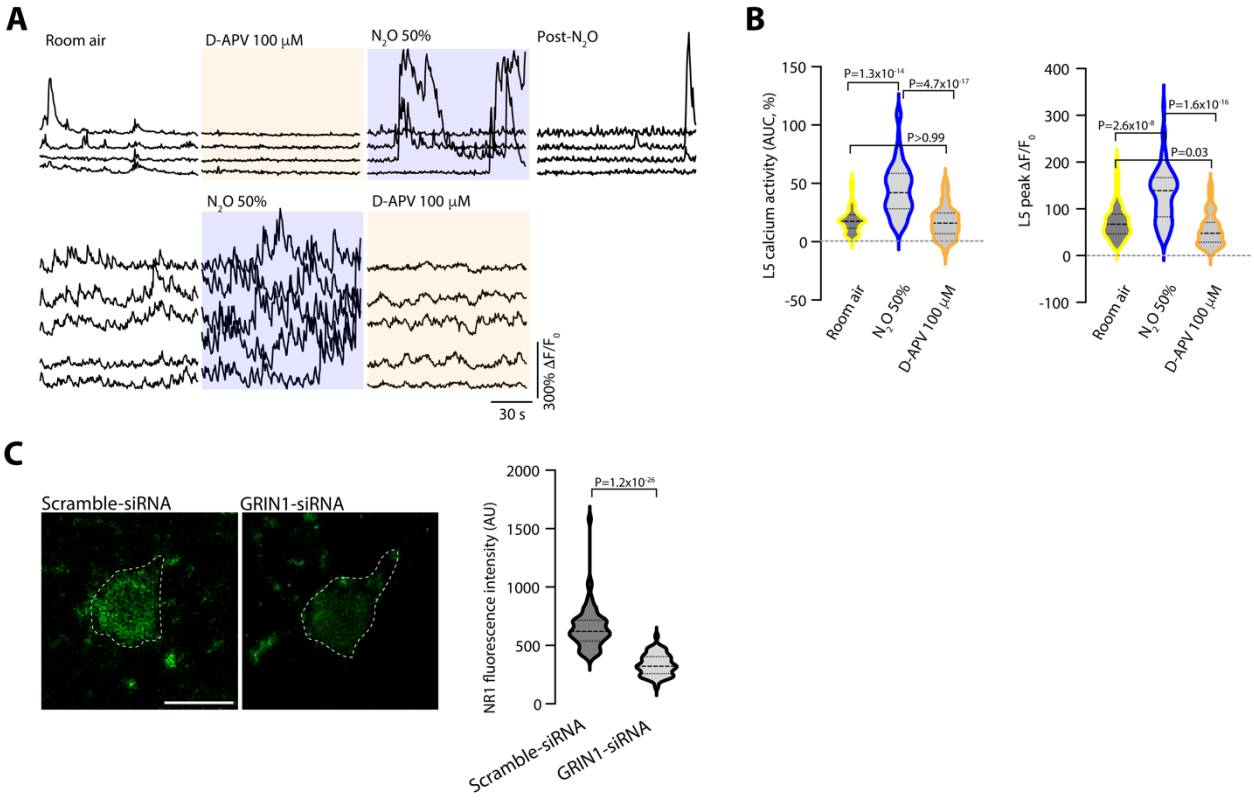

Supplemental Fig. 8. Persistent L5 neuronal activity induced by N_2O reduced by NMDA-receptor inhibition follow exhalation.

A, Top, representative GCaMP6 traces from L5 responses following local application of D-APV (100 μM), N_2O, 1hr after N_2O. N_2O robustly activated these L5 neurons but persistent activity post-N_2O was dampened. Bottom, traces of individual L5 neurons exposed to N_2O and then D-APV. Post-N_2O L5 responses were suppressed in the presence of D-APV.

B, Average calcium activity and peak responses of L5 neurons (n = 81 cells from 3 mice) under room air, N_2O, followed by D-APV. D-APV significantly reduced N_2O-induced responses to baseline measurements (Avg. calcium, Kruskal-Wallis (90): $P = 3.2 \times 10^{-20}$ followed by Dunn's multiple comparisons, $P > 0.99$; Peak calcium, Kruskal-Wallis (73): $P = 1.1 \times 10^{-16}$ followed by Dunn's multiple comparisons, $P = 0.03$).

C, Representative two-photon images (left) and quantification (right) of NR1 fluorescence intensity in cultured cortical neurons infected with either scramble-siRNA (n = 65 cells) or GRIN1-siRNA (n = 56 cells) immunostained against NR1. GRIN1-siRNA significantly reduced NR1 signals (Mann-Whitney rank sum test, $P = 1.2 \times 10^{-26}$). Scale bar, 20 μm.

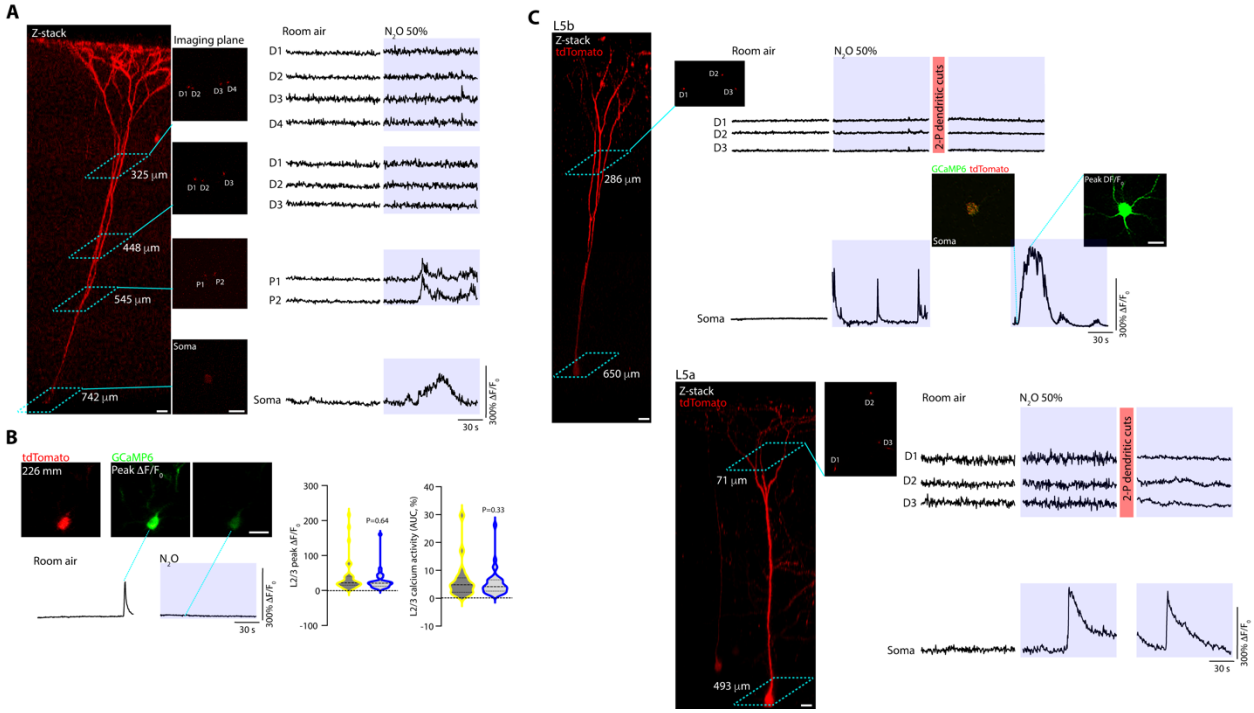

Supplemental Fig. 9. Sparse labelling of individual L5 neurons with GCaMP6 and tdTomato enables two-photon imaging across dendritic compartments to soma.

A, Left, two-photon Z-stack of an individual L5 neuron imaged at several different locations (teal boxes connected to 2-D imaging plane). Right, GCaMP6 traces corresponding to labelled ROIs. N_2O (blue shaded region) recruited L5 soma and deep parent (P) dendrite whereas superficial dendrites (D) remained inactive during the treatment.

B, Left, two-photon images (top) and GCaMP6 traces (bottom) of an individual L2/3 neuron labelled with GCaMP6 and tdTomato. Right, peak and average calcium responses of all individual L2/3 cells recorded (n = 35 from 11 mice) recorded under sparse labelling conditions (dilate CaMK2-Cre; cells/mice different from those reported in Fig. 1 and 2). N_2O inhalation failed to activate these cells over their activity defined in wakefulness/room air (Wilcoxon matched-pairs signed rank: peak calcium, P = 0.64; avg. calcium, P = 0.33).

C, Left, two-photon Z-stack of L5 neuron (top - L5b, bottom - L5a) with two imaging planes marked, one dendritic location with 3 dendritic ROIs and one deep region corresponding to soma. 2 L5 neurons are from 2 different mice. Right, GCaMP6 traces of dendritic ROIs and soma show inactive baseline. N_2O activated the soma without corresponding recruitment of dendrites. Two-photon laser cuts to dendritic ROIs did not change spontaneous somatic responses. Scale bars, 20 µm.

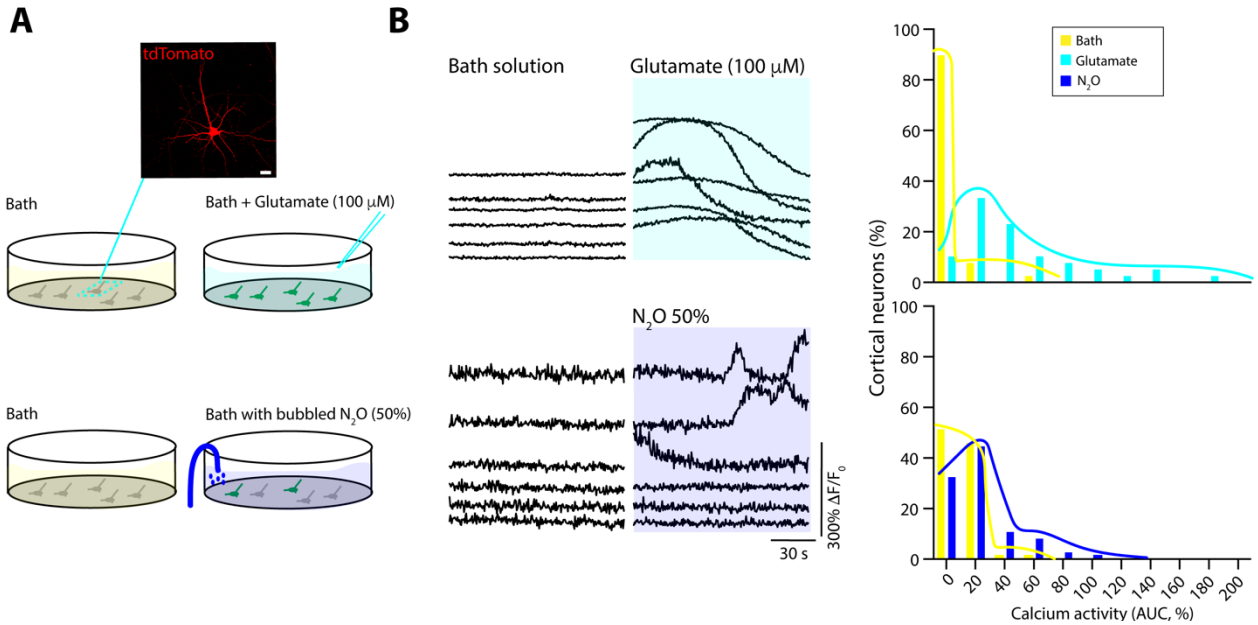

Supplemental Fig. 10. N_2O-induced spontaneous activation of a subset of cortical neurons in vitro. **A**, Schematic of low-density cultured cortical neurons plated on PDL coated glass coverslip recorded under baseline conditions in bath (yellow) followed by either glutamate application (teal) or bubbled N_2O in bath (blue). Top, two-photon image showing sparse platting of pyramidal cell (8 DIV) expressing tdTomato under control of CaMKII promoter. Scale bar, 20 μm.
B, GCaMP6 traces (left) and summary of calcium responses (right) from cortical neurons in bath followed by glutamate application (100 uM) or N_2O. In low-density plating conditions neurons are not spontaneously active (left traces), however glutamate application (top; teal shaded region) induces widespread activation of the entire recorded population (Wilcoxon matched-pairs signed rank test, $n = 39$ from 2 coverslips, $P = 1.8 \times 10^{-8}$). On the other hand, N_2O (bottom; blue shaded region) spontaneously activates a subset of cortical neurons from baseline (Wilcoxon matched-pairs signed rank test, $n = 74$ from 3 coverslips, $P = 2.4 \times 10^{-6}$).

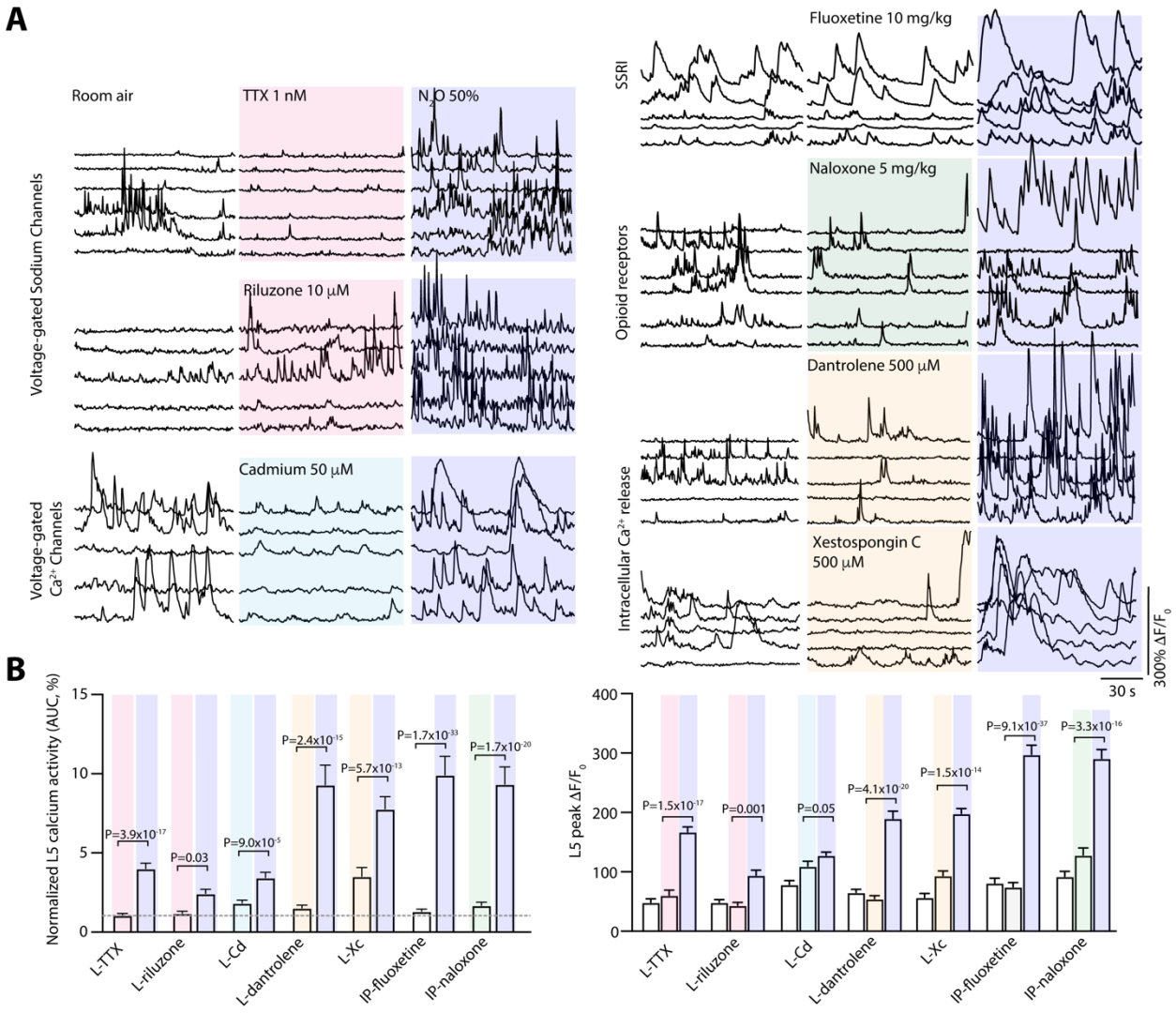

Supplemental Fig. 11. Local pharmacological induced functional attenuation of various channels and receptors prior to N_2O.

A, Representative GCaMP6 traces from individual L5 neurons under room air, either local (L-) or systemic drug administration, followed by N_2O exposure. All drugs were given local except for fluoxetine and naloxone (i.p.). Drug and concentration are noted at middle of each series of traces.

B, Summary of the L5 calcium signals in response to drug manipulation and N_2O. Top, normalized L5 calcium response (Kruskal–Wallis (504): $P = 1.3 \times 10^{-99}$ followed by Dunn's multiple comparisons with exact P values shown; L-TTX, $n = 91$ from 2 mice; L-riluzone, $n = 59$ from 2 mice; L-Cadmium, $n = 109$ from 2 mice; L-dantrolene, $n = 116$ from 3 mice; L-Xc, $n = 122$ from 3 mice; systemic fluoxetine, $n = 144$ from 3 mice; systemic naloxone, $n = 142$ from 3 mice). Bottom, L5 peak $\Delta F/F_0$ (Kruskal–Wallis (818): $P = 2.2 \times 10^{-160}$ followed by Dunn's multiple comparisons with exact P values shown). Voltage sodium and calcium channel blockers reduced N_2O-induced L5 activation but could not block it.

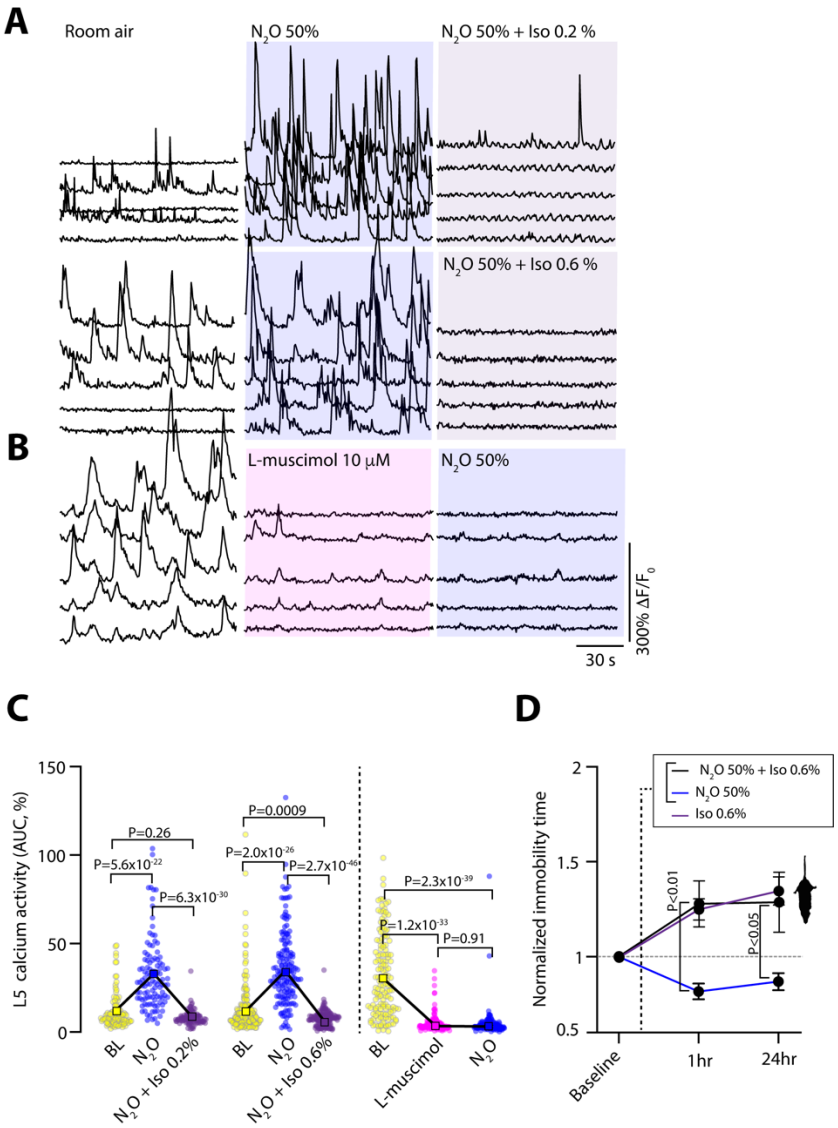

Supplemental Fig. 12. N_2O-induced L5 activity and antidepressant-like effect is occludes by coadministration of GABAergic agents.

A, Representative GCaMP6 traces of individual L5 neuronal responses under room air, N_2O (50%), followed by the N_2O (50%) mixed with isoflurane (Iso; 0.2 or 0.6%).

B, Representative GCaMP6 traces of individual L5 neuronal responses under room air, local application of muscimol (10 uM), followed by the N_2O (50%).

C, N_2O-induced L5 responses are nearly eliminated with both co-inhalation of isoflurane at either concentration (N_2O/Iso 0.2%: n = 108 from 3 mice, Kruskal-Wallis (153): $P = 6.4 \times 10^{-34}$ followed by Dunn's multiple comparisons, $P = 6.3 \times 10^{-30}$; N2O/Iso 0.6%: n = 160 from 4 mice, Kruskal-Wallis (223): $P = 3.5 \times 10^{-49}$ followed by Dunn's multiple comparisons, $P = 2.7 \times 10^{-46}$) or local muscimol (n = 146 from 4 mice, Kruskal-Wallis (216): $P = 1.3 \times 10^{-47}$ followed by Dunn's multiple comparisons, $P = 0.91$)

D, TST immobility time of CORT-treated mice exposed to N_2O 50%, Iso 0.6%, or N_2O 50%/Iso 0.6%. Immobility time of N_2O treated mice (n = 7) were significantly different from Iso (n = 5) or N_2O/Iso (n = 14) at 1 hr (two-way ANOVA: time x treatment $F_{(4, 46)} = 2.6$, $P = 0.002$ post hoc Sidak's test: N_2O vs. Iso $P = 0.0005$, N_2O vs. N_2O/Iso $P = 0.005$) and 24 hr (N_2O vs. Iso $P = 0.002$, N_2O vs. N_2O/Iso $P = 0.04$).

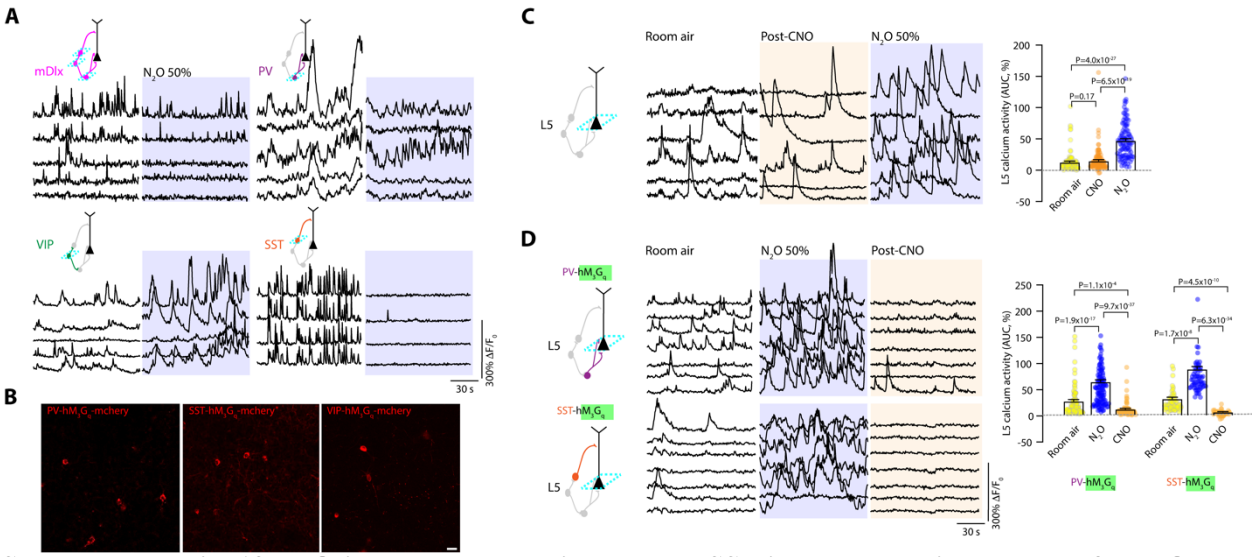

Supplemental Fig. 13. N_2O-induced suppression PV and SST interneurons is necessary for N_2O-induced L5 activity.

A, Representative GCaMP6 traces of genetically defined GABAergic interneurons under room air conditions and N_2O exposure.

B, Two-photon images of PV-, SST-, VIP-expressing interneurons expressing DREADD hM_3G_q-mcherry. Cells imaged in layer 2/3 of Cg1. Scale bar, 20 μm.

C, Representative GCaMP6 traces of individual L5 neurons (left) and all cells avg. calcium response (right; n = 106 cells from 3 mice) recorded under room air, CNO, and N_2O exposure (Kruskal-Wallis (135): $P = 3.9 \times 10^{-30}$ followed by Dunn's multiple comparisons). CNO did not induce a significant change in L5 activity ($P = 0.17$).

D, Left, representative GCaMP6 traces of L5 neurons recorded under room air, N_2O, following CNO injection in interneuron-specific Cre-lines (top – PV, bottom – SST) expressing hM_3G_q in Cg1. N_2O-induced L5 activity is acutely silenced by the activation of PV- or SST-expressing interneurons. Right, summary of all L5 cells recorded. N_2O-induced L5 activity does not persist following activation of either PV (Kruskal-Wallis (169): $P = 1.7 \times 10^{-37}$) or SST (Kruskal-Wallis (149): $P = 3.0 \times 10^{-33}$) neurons. Kruskal–Wallis (one-sided test) followed by Dunn's multiple comparisons shown in panels.

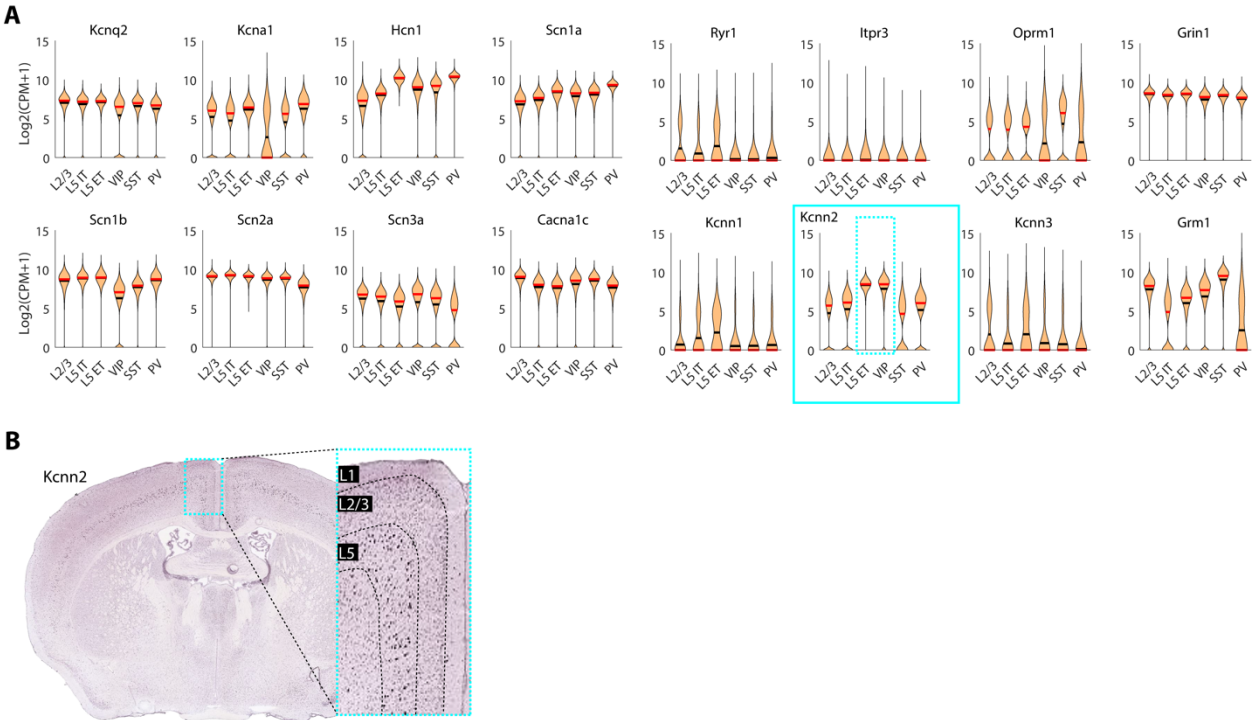

Supplemental Fig. 14. Endogenous SK2 expression in rodent brain is predominantly in layer 5 pyramidal neurons and VIP interneurons.

A, Gene expression levels of candidate channels and receptors (Kcnq2, Kcna1, Hcn1, Scn1a, Scn1b, Scn2a, Scn3a, Cacna1c, Ryr1, Itpr3, Oprm1, Grin1, Kcnn1, Kcnn2, Kcnn3, Grm1) thought to control excitability and calcium dynamics in neuronal cortical cell types (L2/3, L5 IT, L5 ET, VIP, SST, PV; open source whole brain dataset from Allan Brain Cell Atlas, 10x scRNAseq). Distributions of gene expression are shown as violin plots of log2(CPM +1), where black line denotes means, red line denotes medians. CPM = counts per million (transcript reads). Using this screen, we identified the SK2 channel (boxed in teal), encoded by the Kcnn2 gene, to be specifically enriched in Layer 5 ET (extratelencephalic) and VIP neurons (dashed green box) as compared to other cell types (L2/3, L5 IT, SST, PV). Some of these candidates were also empirically confirmed to not block N_2O-induced L5 activity (Supplemental Fig. 11).

B, In situ hybridization of SK2 from Allen Brain mouse atlas shows strong SK2 RNA expression in layer 5 of cortex with sparse labelling in superficial layers. Cortical layers shown in boxed inset.

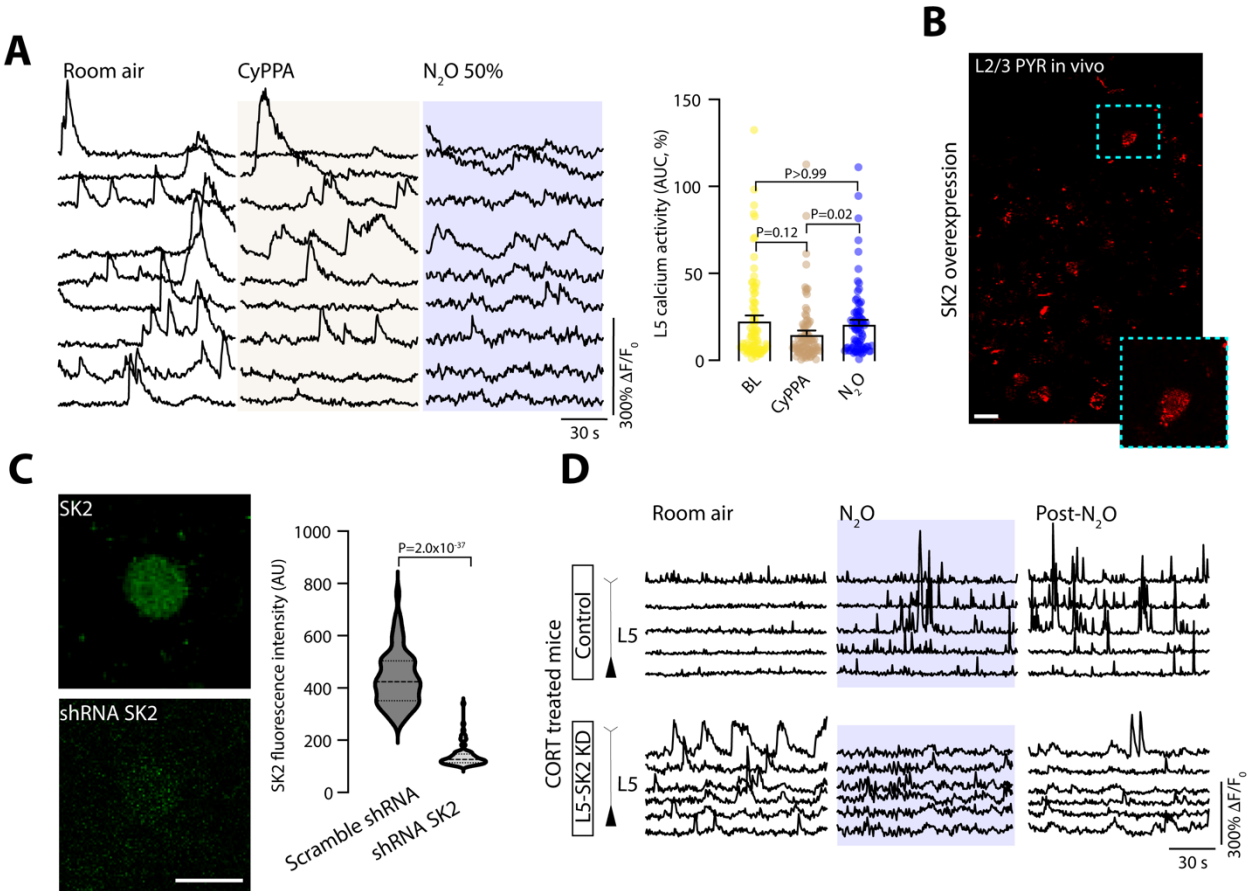

Supplemental Fig. 15. SK2 channel modulation and its impact on N_2O-induced L5 neuronal activity.

A, Representative GCaMP6 traces of individual L5 neurons (left) and all cells avg. calcium response (right; n = 80 cells from 2 mice) recorded under wakefulness, local application of SK2 specific activator, CyPPA, (100 µM, 1 µL), and N_2O exposure. SK2 activation by CyPPA blocked N_2O-induced activation of L5 from baseline wakefulness (Kruskal-Wallis (8): P = 0.02, followed Dunn's comparison between BL and N_2O: $P > 0.99$).

B, Two-photon image of L2/3 neurons overexpressing SK2-mcherry. Scale bar, 20 µm.

C, Two-photon images (left) and fluorescence intensity quantification (right) of cultured cortical neurons immunostained against SK2 under control/scramble shRNA (n = 62 cells) and shRNA-targeted SK2 knockdown (n = 73 cells) conditions. SK2-shRNA significantly reduced SK2 expression signals (Mann Whitney rank sum, $P = 2.0 \times 10^{-37}$). Scale bar, 20 µm.

D, Representative GCaMP6 traces of individual L5 responses from CORT-treated animals under wakefulness, N_2O, following N_2O exposure with normal endogenous SK2 expression (top) and under SK2 knockdown condition (bottom).

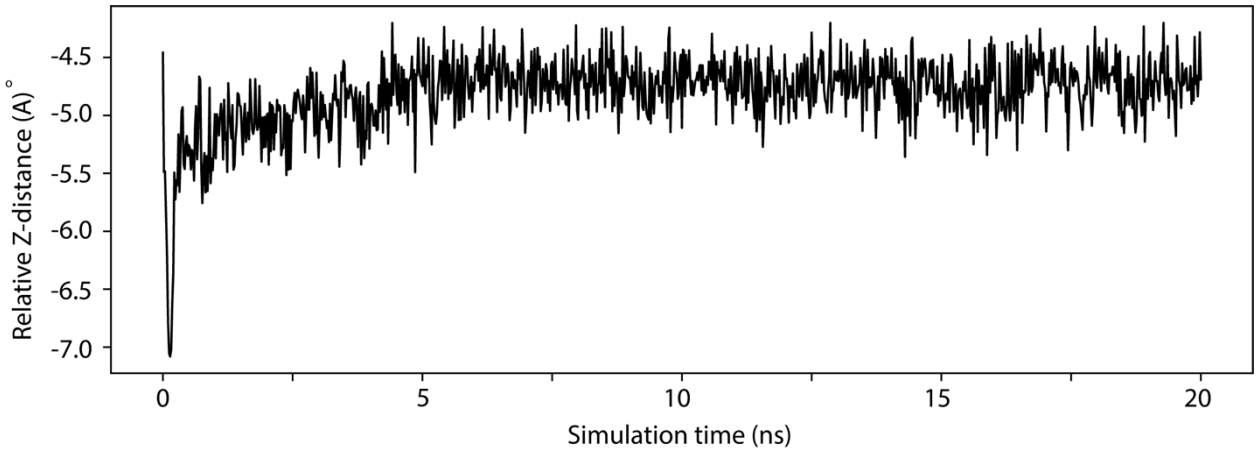

Supplemental Fig. 16. Molecular dynamics simulations of N_2O in SK2 selectivity filter.
Position of N_2O molecule, relative to C-alpha atoms of Tyr361, z-axis component only, as a function of equilibrium MD simulation time. Note the pore axis is parallel to the z-axis.